AIAA JOURNAL
Vol. 39, No. 7, July 2001

Equivalent Skin Analysis of Wing Structures Using Neural Networks

Youhua Liu* and Rakesh K. Kapania†
Virginia Polytechnic Institute and State University, Blacksburg, Virginia 24061

An efficient method of modeling trapezoidal built-up wing structures is developed by coupling, in an indirect way, an equivalent plate analysis (EPA) with neural networks (NN). In the EPA the wing is assumed to behave like a Mindlin plate and is solved using the Ritz method with the Legendre polynomials as the trial functions. The EPA can be made more efficient by avoiding most of the computational effort spent on calculating contributions to the stiffness and mass matrices from every spar and rib. This is accomplished by replacing the wing inner-structure with an "equivalent" material that is combined to the skin and whose properties are simulated by neural networks. The constitutive matrix, which relates the stress vector to the strain vector, and the density distribution of the equivalent material are obtained by enforcing mass and stiffness matrix equivalence with regard to the EPA in a least-squares sense. Neural networks for the material properties are trained in terms of the design variables of the wing structure. Examples show that the present method, which can be called an equivalent skin analysis (ESA) of the wing structure, is more efficient than the EPA, and still fairly good results can be obtained. The present ESA is very promising to be used at the early stages of wing structure design.

Introduction

TRADITIONALLY, the conceptual design is often carried out using simplified relations that have been learned from previous similar designs. This approach can only result in incremental advancements in technology because experience-based design makes large step design extrapolations too risky. This risk can be reduced significantly if the design is based on physics-based high-fidelity models because using these models one can predict the consequences of large design extrapolations with a greater confidence.

Physics-based, high-fidelity models, such as those in the finite element analysis (FEA) for structures, computational fluid dynamics for aerodynamic loads, etc., are increasingly being used as early as possible in airplane design. This is not surprising because it is estimated that about 90% of the cost of a product is committed during the first 10% of the design cycle, and an accurate analysis is often crucial to obtaining a good estimate of the manufacturing and life-cycle costs of a product.

For structural analysis the finite element method (FEM) is widely used because of its generality, versatility, and reliability, but its use in the early design stages faces some major obstacles: a prohibitive preparation time for the FE model data and a large amount of CPU time for problems with a high number of degrees of freedom. This is especially true for complex built-up structures such as an airplane wing.

In the aerospace engineering community several efficient methods have been developed for dealing with this situation, one of which is the equivalent plate modeling.[1] A detailed description of the equivalent plate methodology development and literature can also be found in Ref. 2. In a previous effort of the present study, Kapania and Liu[1] have developed an equivalent plate analysis (EPA) method for efficiently calculating the static and vibration problems of general trapezoidal built-up wing structures composed of skins, spars, and ribs. Details of the method can be found in Ref. 1 and will be briefed in the following section.

But there is a problem in the method in Kapania and Liu,[1] that is, because complex trial functions are used, the stiffness and mass matrices are hard to be integrated analytically, as in the case of Livne,[3] and numerical integration over every item of the structural components takes a large part of the computing effort. For instance, in solving a free vibration problem, evaluating various matrices requires about $\frac{2}{3}$ of the total CPU time.

This problem can be addressed by representing the wing inner structure by equivalent skins or a shear-carrying core, that is, by "smearing" those components into the skins or a more uniform core. In Lynch et al.,[4] the caps of spars of a YF16 wing are represented by an equivalent skin. The idea of replacing the shear webs in a wing plate model by an equivalent sandwich core was discussed in Livne.[3] In the present paper it is attempted to develop a method in which evaluation of matrices is performed only over the skins, whose equivalent material constitutive matrix and mass density distribution are changed accordingly to incorporate the spar and rib effects. For the purpose of design optimization, the new skin material properties are simulated using neural networks in terms of the wing design variables. As shall be shown, whereas the new method, which will be called equivalent skin analysis (ESA) hereafter, gives almost equally good results, it uses only a fraction of the CPU time spent in the ordinary EPA in evaluating the matrices.

EPA Method

We want to analyze a trapezoidal wing by assuming that it behaves as a plate whose deformation satisfies the Reissner–Mindlin displacement field, which is a first-order shear deformation theory.[1] For the convenience of calculation, a coordinate transformation from (x, y) to (ξ, η) is performed, which transforms the wing plan surface from the original trapezoidal to a square. Details of the coordinate transformation are available in Ref. 1.

By representing the displacement components as the sum of terms $P_{i-1}(\xi)P_{j-1}(\eta)$, where P are the Legendre polynomials, $i = 1, \ldots, I$, $j = 1, \ldots, J$ (I, J are integers), we can call the vector composed of all of the coefficients of the terms as the generalized displacement vector. Based on this displacement vector and considering the total strain and kinetic energy of the wing structure, we can derive the stiffness and mass matrices as in the following forms:

$$[K] = \iiint_V [C]^T[T]^T[D][T][C]\,\mathrm{d}V \tag{1}$$

$$[M] = \iiint_V \rho[H]^T[ZZ][H]\,\mathrm{d}V \tag{2}$$

where the integration domain V includes all and only the spaces that the components of the wing occupy and $[D]$ and ρ are the material

Received 16 January 2000; revision received 22 January 2001; accepted for publication 2 February 2001.

*Research Assistant, Department of Aerospace and Ocean Engineering. Member AIAA.
†Professor, Department of Aerospace and Ocean Engineering. Associate Fellow AIAA.

constitutive matrix and density, respectively. Details of matrix $[C]$, $[T]$, $[H]$, and $[ZZ]$ can be found in Ref. 1. The integration in the (ξ, η) plane is performed using the Gaussian quadrature.[1]

The boundary conditions are approximated by applying springs with very large magnitudes of stiffness on the boundaries. An integration on the boundaries gives$[K_{\text{spring}}]$[1]. The total stiffness and mass matrices of the wing structure are given as

$$[K_{\text{total}}] = [K_{\text{strain}}] + [K_{\text{spring}}]$$

$$[K_{\text{strain}}] = [K_{\text{skin}}] + [K_{\text{spar}}] + [K_{\text{rib}}] \tag{3}$$

$$[M_{\text{total}}] = [M_{\text{skin}}] + [M_{\text{spar}}] + [M_{\text{rib}}] \tag{4}$$

The natural frequencies and mode shapes for the free vibrating wing can be determined by applying the Lagrange's equations, which result in the following eigenvalue problem:

$$[K_{\text{total}} - \lambda M_{\text{total}}]\{x\} = 0 \tag{5}$$

where $\lambda = \omega^2$ is an eigenvalue of the system of equations, ω is the corresponding frequency in radians/second, and $\{x\}$ is the corresponding eigenvector.

Static problems (including stress distributions) can be readily solved by making use of the total stiffness matrix $[K_{\text{total}}]$. For details one can refer to Ref. 1.

Compared with the approaches in Kapania and Lovejoy[5] and Cortial,[6] the formulation in Ref. 1 is such that there is no limitation on the wing thickness distribution. As shown in Ref. 1, the method shows a good performance for both static and vibration problems in comparison with the FEA using MSC/NASTRAN.

Application of Neural Networks in Structural Problems

Neural network (NN)[7] has found numerous applications in science and engineering. In the field of structural engineering, there have been a lot of attempts and researches making use of NN to improve efficiency or to capture relations in complex analysis and design problems. The following are a few examples. Hajela and Berke[8] gave an overview of the neural computing approach and examined the role of neural computing strategies in structural analysis and design. Abdalla and Stavroulakis[9] applied NN to represent experimental data to model the behavior of semirigid steel structure connections, which are related to some highly nonlinear effects such as local plastification, etc. Several cases of NN application in structural engineering can be found in Vanluchene and Sun,[10] all of which were later restudied in Gunaratnam and Gero[11] with a conclusion that representational change of a problem based on dimensional analysis and domain knowledge can improve the performance of the networks. In Liu et al.[12] methodologies of applying NN and genetic algorithms to simulate and synthesize substructures were explored in the solution of one- and two-dimensional beam problems.

For the efficient simulation of the structural performances of complex wings, generally there can be two directions to apply NN. One way is to use NN to simulate directly the structural responses calculated using various methods, but according to Ref. 11, this is not the best use of the NN in structural engineering: "The real usefulness of neural networks in structural engineering is not in reproducing existing algorithmic approaches for predicting structural responses, as a computationally efficient alternative, but in providing concise relationships that capture previous design and analysis experiences that are useful for making design decisions."

In the present study an indirect way of applying the NN is pursued. In the EPA of a complex wing, the computation effort is mainly spent on integrals for generating the contribution from the inner-structural components of the wing, the spars and the ribs, to the stiffness and mass matrices. If an equivalent anisotropic material can be found to replace the inner components in terms of an equivalent skin such that the new composite wing has similar global properties as the original one, then the EPA can be performed more efficiently. Solution of the adequate material properties of the anisotropic material is the major obstacle here. The role of the NN will be to relate the material properties to all kinds of wing design parameters, when there exists enough database for training.

ESA of Wing Structures

It is desired to replace the actual wing structure by an equivalent continuum model, that is, one that is composed of a skinlike material, whose constitutive matrix $[D]$ and distribution of mass in Eqs. (1) and (2) are to be decided. Flowcharts of ESA in comparison with EPA[1] are shown in Fig. 1. Because "NN retrieval of $[D]$ and ρ" needs almost no computational cost, once the networks for $[D]$ and ρ are trained, ESA only requires the calculation of the skins to obtain the total $[K]$ and $[M]$.

It is assumed that the mass density ρ is a function of position in the planform, whereas each term of $[D]$ is a constant throughout the wing area. There can be other choices, as will be discussed later.

We are going to solve the preceding problem by requiring that the stiffness and mass matrices of the equivalent model are most approximate to those of the actual wing in a least-squares sense. This gives the following procedures.

Constitutive Matrix

Let us write $[K] = [K_{\text{strain}}] = [K_{ij}]$ as the target matrix, and the stiffness matrix of the equivalent continuum model is

$$[\tilde{K}] = \sum_m \sum_n g_m g_n [C]^T_{mn} [T]^T_{mn} [D][T]_{mn} [C]_{mn} = [\tilde{K}_{ij}]$$

$$= \left[\sum_p \sum_q D_{pq} \left(\sum_m \sum_n \tilde{G}^{ij}_{pq,mn} \right) \right] = \sum_{p,q} D_{pq} \left[G^{ij}_{pq} \right] \tag{6}$$

where g_m and g_n are the Gauss quadrature weights; the constitutive matrix $[D]$ relates the stress and strain vectors by $\{\sigma\} = [D]\{\varepsilon\}$;

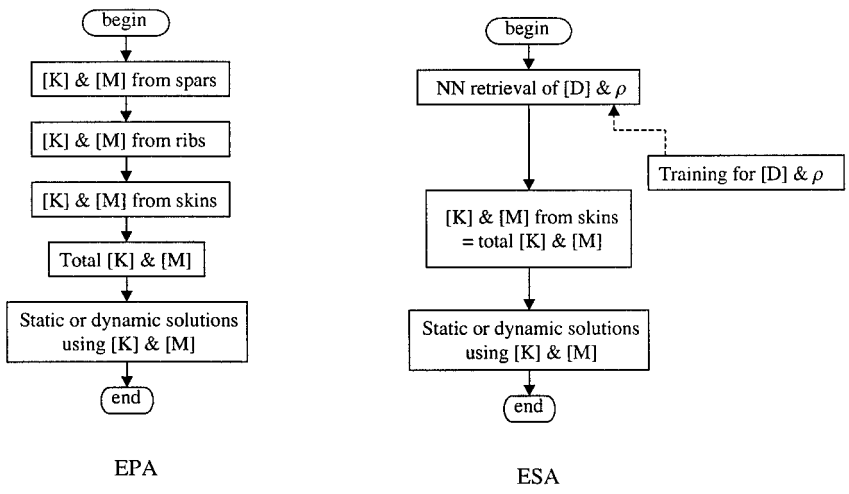

Fig. 1 Flowcharts for EPA and ESA.

and D_{pq} is the pth row, qth column term of the constitutive matrix; m ($m = 1, \ldots, K$) corresponds to the mth Gauss integration position in the x direction, K is an integer with a usual value of 6 or 8; n ($n = 1, \ldots, K$) corresponds to the nth Gauss integration position in the y direction; $p = 1, \ldots, 5$ is the row number of $[D]$; $q = 1, \ldots, 5$ is the column number of $[D]$;

$$\bar{G}^{ij}_{pq,mn} = g_m g_n [C]^T_{mn} [T]^T_{mn} \begin{bmatrix} & & 0 & & \\ & & \vdots & & \\ 0 & \cdots & 1 & \cdots & 0 \\ & & \vdots & & \\ & & 0 & & \end{bmatrix}^{\begin{matrix}1\\ \vdots \\ p\\ \vdots \\ 5\end{matrix}} [T]_{mn}[C]_{mn}$$

$$\begin{matrix} & & 1 & & 5 \\ & & \cdots & & \\ & & q & & \\ & & \cdots & & \\ & & 5 & & \end{matrix}$$

$$G^{ij}_{pq} = \sum_{m,n} \bar{G}^{ij}_{pq,mn} \tag{7}$$

By constructing an error function

$$E_K = \sum_{i,j} w^K_{ij} [\tilde{K}_{ij}(D_{pq}) - K_{ij}]^2 \tag{8}$$

where w^K_{ij} are the weight coefficients, and by requiring

$$\frac{\partial E_K}{\partial D_{pq}} = 2 \sum_{i,j} w^K_{ij} [\tilde{K}_{ij}(D_{pq}) - K_{ij}] \frac{\partial \tilde{K}_{ij}}{\partial D_{pq}} = 0$$

and noting

$$\frac{\partial \tilde{K}_{ij}}{\partial D_{pq}} = G^{ij}_{pq}$$

(G^{ij}_{pq} means the i, j-th term of matrix $[G_{pq}]$), we can obtain the constitutive matrix term $[D_{pq}]$ by solving the following linear equation set:

$$\sum_{p',q'} \left(\sum_{i,j} w^K_{ij} G^{ij}_{p'q'} G^{ij}_{pq} \right) D_{p'q'} = \sum_{i,j} w^K_{ij} K_{ij} G^{ij}_{pq}$$

$$i, j = 1, \ldots, K, \qquad p, q, p', q' = 1, \ldots, 5 \tag{9}$$

This is an equation set with 25 unknowns. Because $i, j = 1, \ldots, N$ and $N = 5K^2$ is usually very large (if we use the Legendre polynomials of six terms as the basis functions, $N = 180$; if eight terms are used, then $N = 320$), the job of generating the matrix in Eq. (9) will be very extensive.

If $[D]$ is assumed to be symmetrical, then Eq. (9) will become

$$\sum_{(p',q')} \left\{ \sum_{i,j} w^K_{ij} \left[G^{ij}_{p'q'} + (1 - \delta_{p'q'}) G^{ij}_{q'p'} \right] G^{ij}_{pq} \right\} D_{p'q'} = \sum_{i,j} w^K_{ij} K_{ij} G^{ij}_{pq} \tag{10}$$

where (p', q') and (p, q) have the following 15 instead of 25 combinations: (1,1), (1,2), (1,3), (1,4), (1,5), (2,2), (2,3), (2,4), (2,5), (3,3), (3,4), (3,5), (4,4), (4,5), and (5,5).

Mass Distribution

Let us write $[M] = [M_{\text{total}}] = [M_{ij}]$ as the target matrix, and

$$[\tilde{M}] = \sum_m \sum_n \rho_{mn} g_m g_n [H]^T_{mn} [Z]^T_{mn} [Z]_{mn} [H]_{mn} = \sum_m \sum_n \rho_{mn} [F]_{mn} \tag{11}$$

as the mass matrix of the continuum model, where m ($m = 1, \ldots, K$) corresponds to the mth Gauss integration position in the x direction; n ($n = 1, \ldots, K$) corresponds to the nth Gauss integration position in the y direction; ρ_{mn} is the mass density of the equivalent model at position (m, n); g_m and g_n are integration weights; and $[F]_{mn} = [H]^T_{mn} [Z]^T_{mn} [Z]_{mn} [H]_{mn}$ is a $N \times N$ matrix varying with position (m, n).

By constructing an error function

$$E_M = \sum_{i,j} w^M_{ij} [\tilde{M}_{ij}(\rho_{mn}) - M_{ij}]^2 \tag{12}$$

where w^M_{ij} are weight coefficients, and by requiring

$$\frac{\partial E_M}{\partial \rho_{mn}} = 2 \sum_{i,j} w^M_{ij} [\tilde{M}_{ij}(\rho_{mn}) - M_{ij}] \frac{\partial \tilde{M}_{ij}}{\partial \rho_{mn}} = 0$$

and noting

$$\frac{\partial \tilde{M}_{ij}}{\partial \rho_{mn}} = F^{ij}_{mn}$$

(F^{ij}_{mn} is the i, jth term of matrix F_{mn}), we can obtain the mass distribution ρ_{mn} by solving the following linear equation set with K^2 unknowns:

$$\sum_{m',n'} \left(\sum_{i,j} w^M_{ij} F^{ij}_{m'n'} F^{ij}_{mn} \right) \rho_{m'n'} = \sum_{i,j} w^M_{ij} M_{ij} F^{ij}_{mn}$$

$$m, n = 1, \ldots, K, \qquad m', n' = 1, \ldots, K \tag{13}$$

In the present study the following weight coefficients are used:

$$w^K_{ij} = 10 \left| K^{\text{Skin}}_{ij} \right| \Big/ \max_{i,j} \left(\left| K^{\text{Skin}}_{ij} \right| \right) + 1$$

$$w^M_{ij} = 10 \left| M^{\text{Skin}}_{ij} \right| \Big/ \max_{i,j} \left(\left| M^{\text{Skin}}_{ij} \right| \right) + 1 \tag{14}$$

The basic idea behind this choice is that we want to form the equivalent matrices more in the way of the skin's, which is more like a plate than the other components of the wing.

Several choices about the variation of ρ and $[D]$ have been tried, but it is found that the present assumptions give the best results in terms of feasibility and accuracy. For instance, to be consistent with the assumption that each term of $[D]$ is a constant throughout the wing area, ρ can also be assumed a constant. This certainly decreases the accuracy of the method as a result of the loss of flexibility in varying ρ to simulate the target mass matrix $[M]$, but the resultant reduction in computational effort is small because in the first place forming Eq. (13) and training the ρ-related neural networks do not need much CPU time. In other cases $[D]$ was assumed to be variable in the spanwise direction or throughout the wing area, but it was found that although the equivalent material is more flexible to simulate the target stiffness matrix $[K]$ the resultant $[\tilde{K}]$ usually has a larger abstract error and the solution of the free vibration problem usually gives worse natural frequencies. Moreover, the CPU time needed for generating Eq. (10), which requires the major computational effort in our method, increases in a factor of about K (number of Gauss integration points, usually with a value of 6–8) in the case of $[D]$ being variable in the spanwise direction. In the case of $[D]$ being variable throughout the wing area, the increase can be as large as K^2 times. As we shall see in the following examples, these kinds of increase in CPU time are formidable.

Examples and Discussion

The NN-aided equivalent plate analysis, or briefly ESA method, is compared with the ordinary EPA[1] in three cases where four to six design variables are involved respectively. Design variables for wing structure can be sizing-type variables (skin thickness, spar or rib sectional area, etc.), shape variables (the plan surface dimensions and ratios), and topological variables (total spar or rib number, wing topology arrangements etc.). In some of the results, FEA results employing MSC/NASTRAN are also provided as a benchmark.

Some common parameters of the built-up wing structures will be specified herein if not specified otherwise in the following cases. The sections were generated by the Karman–Trefftz transformation.[13] The section thickness-chord ratio varies from 0.15 at the root

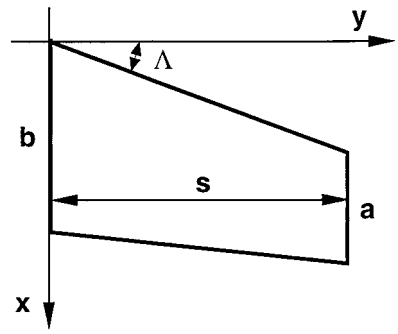

Fig. 2 Plan configuration of a trapezoidal wing: $A = \frac{1}{2}s(a+b)$, $\alpha = s^2/A$, $\tau = a/b$.

to 0.06 at the tip. Skin thickness $t_0 = 0.118$ in.; spar cap height $h_1 = 0.197$ in.; spar cap width $l_1 = 0.373$ in.; spar web thickness $t_1 = 0.058$ in. (for definition of h_1, etc., see Ref. 1); the ribs have the same cap dimensions and web thickness as the spars. Mass density $\rho = 2.526 \times 10^{-4}$ lb $\cdot$ s^2/in.^{4}, Young's modulus $E = 1.025 \times 10^7$ lb/in.^{2}, Poisson's ratio $\nu = 0.3$. The wing is clamped at the root.

Four-Variable Case: Design Space I

In this case, 4 spars and 10 ribs are evenly distributed inside the wing planform under the skins. For a trapezoidal wing there are four major independent shape variables: sweep angle Λ, aspect ratio α, taper ratio τ, and plan area A (Fig. 2). A 3^4 full factorial experimental design with three levels in Λ, α, τ, and A, respectively, was used. Particulars of the levels of every variable are as follows:

$$\Lambda = \{0, 15, 30 \text{ deg}\}, \qquad \alpha = \{1.0, 1.75, 2.5\}$$

$$\tau = \{0.3, 0.45, 0.6\}, \qquad A = \{2000, 3500, 5000\} \text{ in.}^2$$

For each point in this design space, the EPA is carried out, then Eqs. (10) and (13) are used to generate the 15 constitutive matrix terms and mass densities at 36 (6×6) Gauss sampling points, and the ESA is performed. For each of these parameters, a feedforward NN with a structure of $4 \times 15 \times 10 \times 1$, i.e., 4 inputs, 15 neurons in the first hidden layer, 10 neurons in the second hidden layer, and 1 output, was trained using the MATLAB® NN Toolbox function trainlm that trains feedforward network with the Levenberg–Marquardt algorithm.[10] Therefore, there are totally $15 + 36 = 51$ networks to be trained. There are 81 (3^4) sets of training data, which are nondimensionalized before the training process. Once the networks are trained, the input–output relationships can be readily retrieved by using the MATLAB® function simuff.

The major computational effort was spent in generating the 81 sets of training data, with about 45 hours of CPU time being spent on a PII/350 personal computer, whereas less than 1 hour of CPU time being used in training the neural networks. A set of results are given in Fig. 3, where 25 points, which mean 25 new designs, were randomly chosen within the design space box. Upon each new design both the EPA and the ESA are performed. The planforms of the new design are shown in Fig. 3a. The first 10 natural frequencies by the EPA and the ESA are compared in Fig. 3b, and their relative differences (based on the EPA results) are shown in Fig. 3c. It can be seen that except for a very few cases (3 out of 250), the relative difference is within −10–10%.

Figure 4a shows 16 new designs through a randomly chosen path inside the design space box, which is defined as

$$v^j = v_0^j(1 - a^j) + v_1^j a^j, \qquad j = 1, \ldots, 4$$

$$v^1 = \Lambda, \qquad v^2 = \alpha, \qquad v^3 = \tau, \qquad v^4 = A$$

$$a^j = s^{n_j}, \qquad n_j = r_j/(1 - r_j) \tag{15}$$

where v_0^j and v_1^j are the lower and upper bounds of variable v^j, for instance, $v_0^1 = 0$ deg, $v_1^1 = 30$ deg, etc., $s \in [0, 1]$ is the range of a shape variable, and r_j ($j = 1, \ldots, 4$) are randomly determined

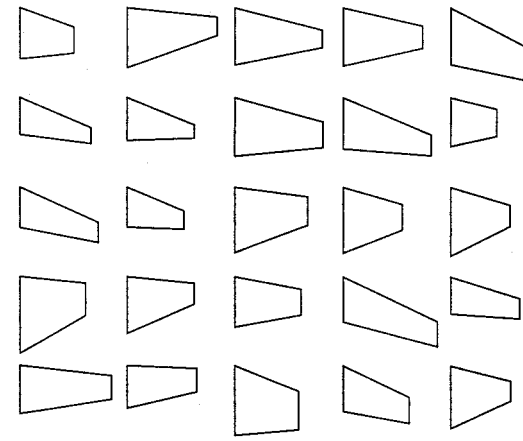

Fig. 3a Twenty-five randomly chosen wing planforms in design space I.

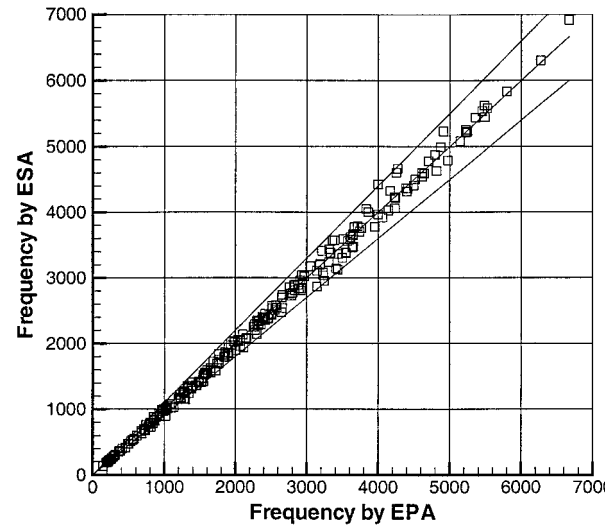

Fig. 3b Comparison of the first 10 frequencies by EPA and ESA.

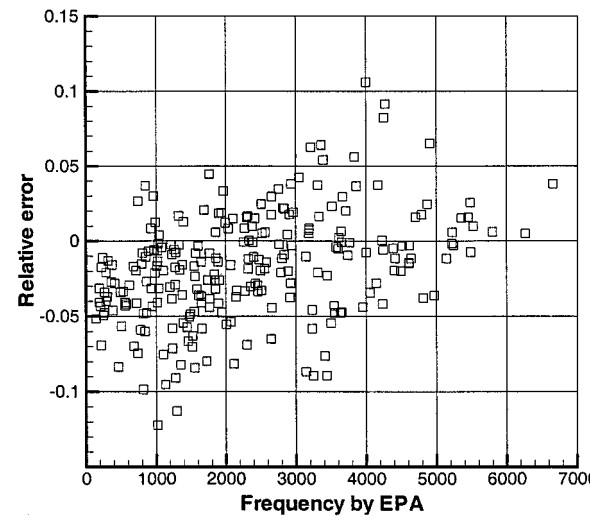

Fig. 3c Relative errors ($\{f_{ESA} - f_{EPA}\}/f_{EPA}$) in Fig. 3b.

values between 0 and 1. Results of natural frequencies of the first six modes for wing structures defined by points along a path with $n_1 = 0.945$, $n_2 = 8.200$, $n_3 = 3.203$, and $n_4 = 1.778$ are shown in Fig. 4b, where it can be seen that results by the EPA and the ESA agree with each other quite well.

Whereas Figs. 3 and 4 are about free vibration frequencies, Fig. 5 shows some static results. For an arbitrary new design whose planform is shown in Fig. 6a, a downward ($-z$ direction) point force of

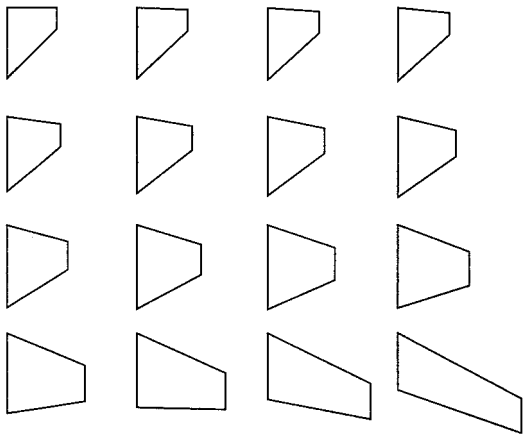

Fig. 4a Sixteen wing planforms systematically varying through design space I.

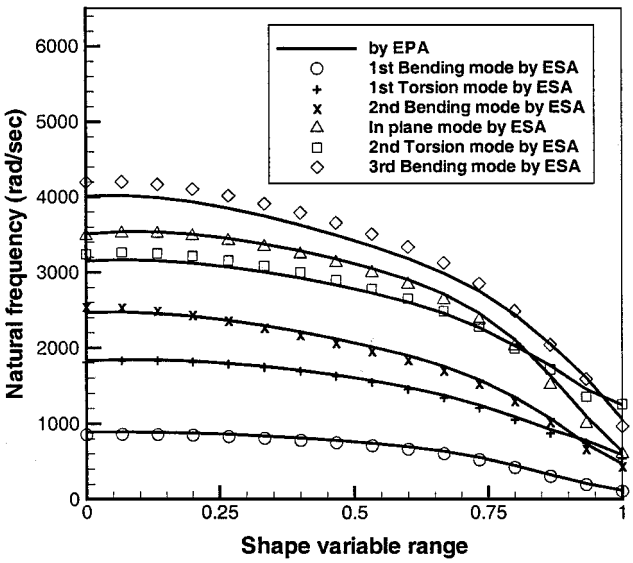

Fig. 4b Comparison of the first six frequencies by EPA and ESA.

1 lb is applied at the midpoint of the wing tip. (Actually the force is divided into components acting on the two spar tips close to the midpoint.) Figure 5a shows displacements along the leading edge by the EPA and the ESA, where u, v, w are displacement components in the chordwise, spanwise, and vertical directions, respectively. Figures 5b and 5c show the Von Mises stress distributions at the wing root and the central spanwise line, respectively. It can also be seen that the EPA and the ESA give very comparable results for the static case.

Six-Variable Case: Design Space II

In this case spars and ribs are evenly distributed inside the wing planform, but their numbers are design variables. A 3^6 full factorial experimental design with three levels in Λ, α, τ, A, and numbers of spars and ribs n_{spar} and n_{rib}, respectively, was used. Particulars of the levels of every variable are as follows:

$$\Lambda = \{0, 15, 3\,\text{deg}\}, \qquad \alpha = \{1.0, 1.75, 2.5\}$$

$$\tau = \{0.3, 0.45, 0.6\}, \qquad A = \{2000, 3500, 5000\}\,\text{in.}^2$$

$$n_{\text{spar}} = \{2, 4, 6\}, \qquad n_{\text{rib}} = \{7, 10, 13\}$$

Similar to case I, the 51 feedforward NN representing the constitutive matrix terms and mass densities with a structure of $6 \times 15 \times 10 \times 1$ were trained using the MATLAB® NN Toolbox. There are 729 (3^6) sets of data that could be used for training, but it was found that at some design points the differences between the natural frequencies by the EPA and the ESA become too large.

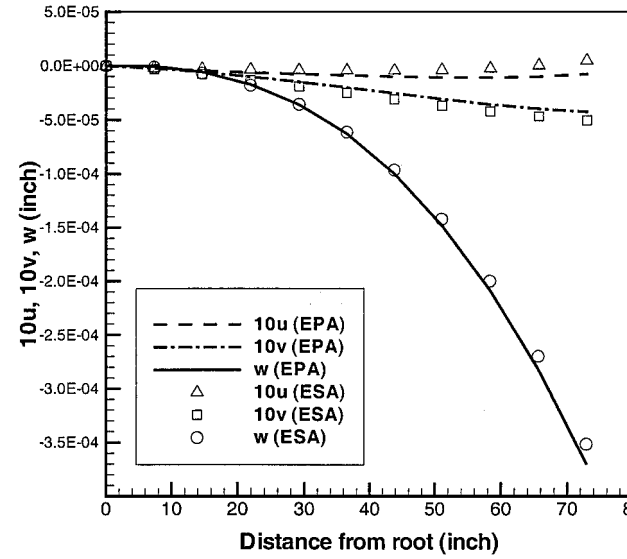

Fig. 5a Comparison of displacements by EPA and ESA under 1-lb tip force.

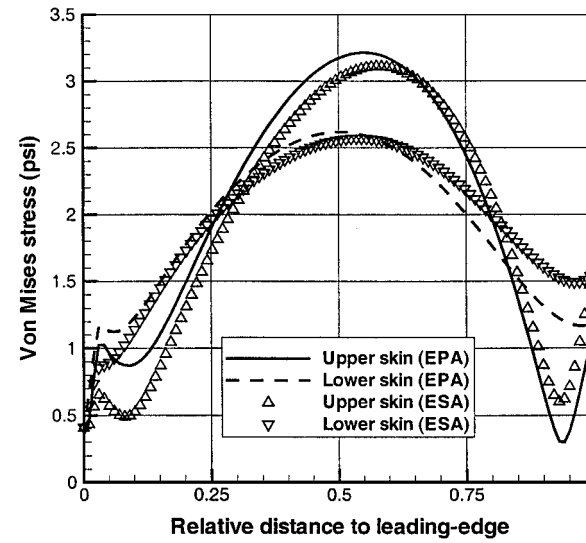

Fig. 5b Comparison of the Von Mises stress at wing root by EPA and ESA under 1-lb tip force.

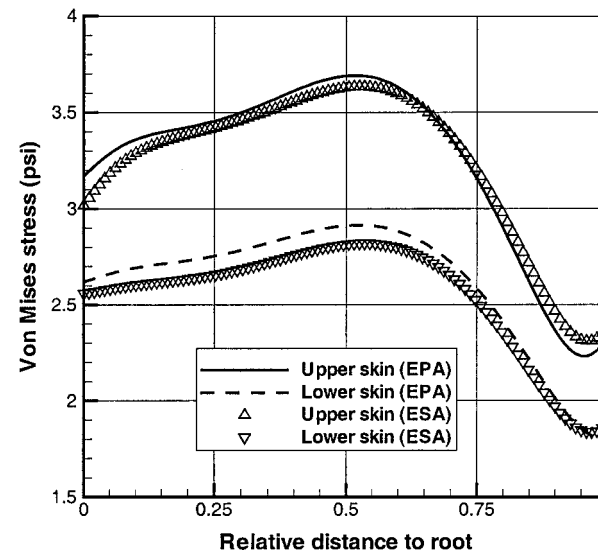

Fig. 5c Comparison of the Von Mises stress along central spanwise line by EPA and ESA under 1-lb tip force.

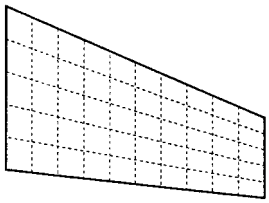

Fig. 6a Arbitrarily chosen wing planform in design space I and II.

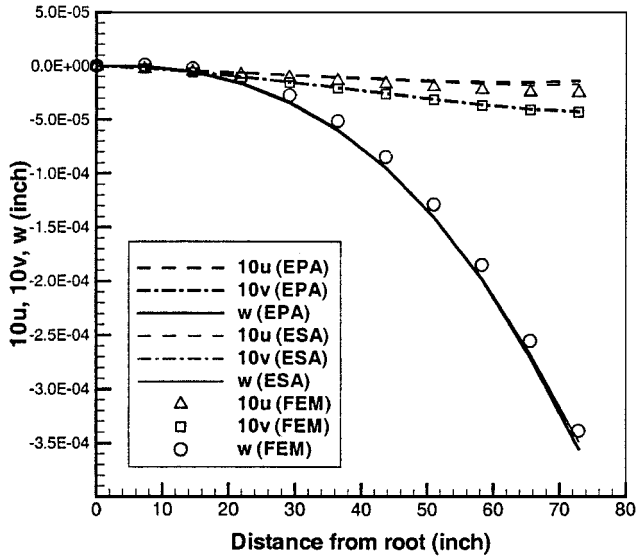

Fig. 6b Comparison of displacements by EPA and ESA under 1-lb tip force.

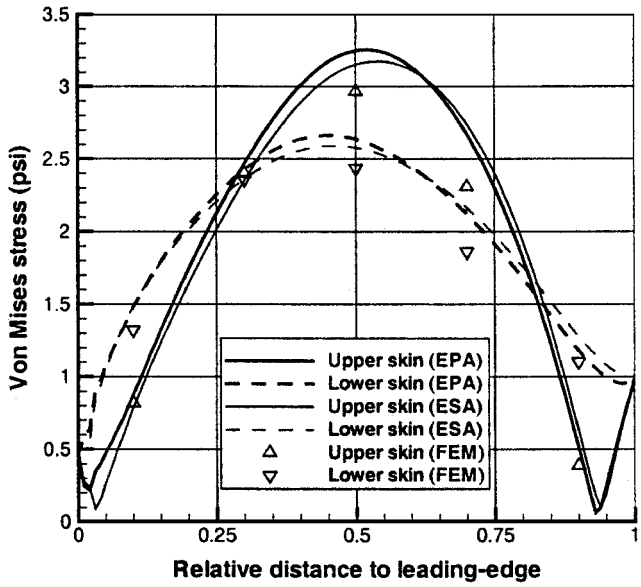

Fig. 6c Comparison of the Von Mises stress at wing root by EPA and ESA under 1-lb tip force.

Therefore, a screening process was introduced, in which any point where the maximum relative difference between the first 10 natural frequencies by the EPA and the ESA surpasses 20% would be discarded. This led to the removal of 28 points through the process; therefore, 701 sets of data were used for training.

Generating the 729 sets of pretraining data used about 152 hours of CPU time on the Crunch (SGI Origin 2000 with eight R10000 processors) of the College of Engineering, Virginia Tech, and training the neural networks spent about 2 hours on a PII/350 PC. A set of results are given in Fig. 7, where 25 points were randomly chosen within the design space box. The planforms of the new designs are shown in Fig. 7a, where dashed lines indicate the spar or rib positions. The first 10 natural frequencies by the EPA and the ESA

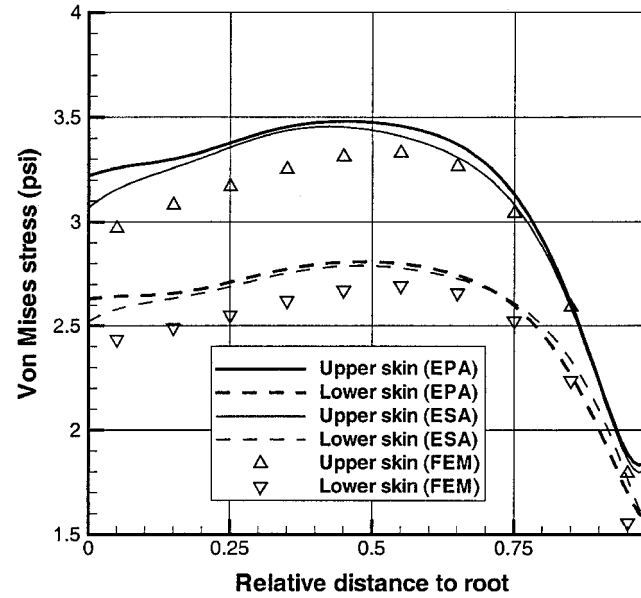

Fig. 6d Comparison of the Von Mises stress along central spanwise line by EPA and ESA under 1-lb tip force.

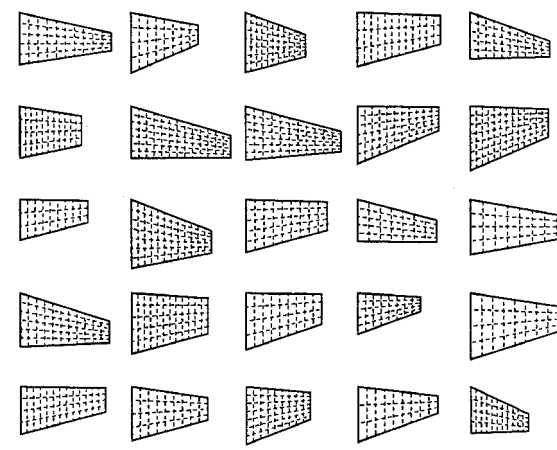

Fig. 7a Twenty-five randomly chosen wing planforms in design space II.

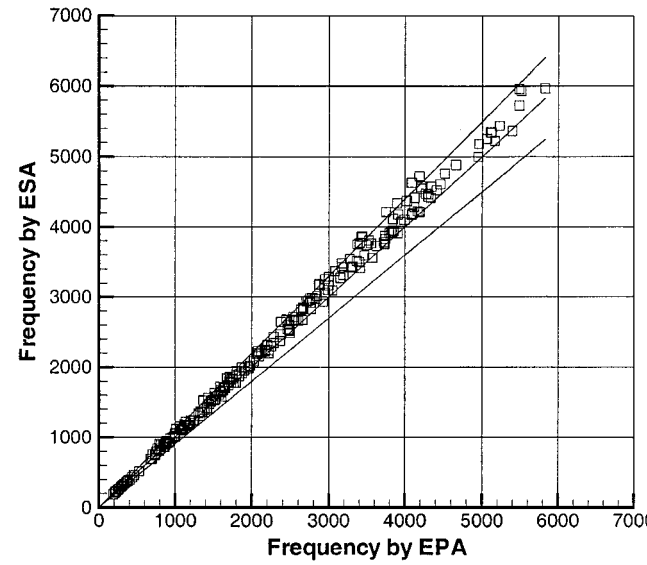

Fig. 7b Comparison of the first 10 frequencies by EPA and ESA.

Table 1 Natural frequencies of the wing in Fig. 6a

Mode shape and number	Frequency, rad/s		
	EPA	ESA	FEM
1st bending, 1	279.3	274.5	279.9
2nd bending, 2	982.8	984.1	965.6
1st torsion, 3	1057.5	1045.1	973.5
In plane, 4	1447.4	1440.3	1454.4
2nd torsion, 5	1945.5	1936.3	1830.8

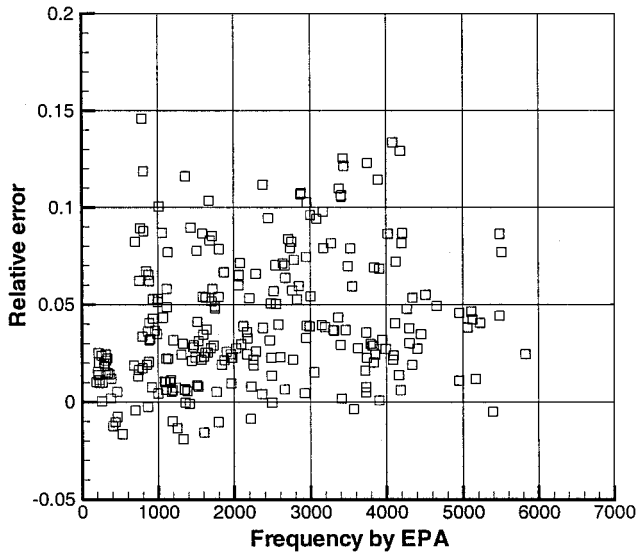

Fig. 7c Relative errors ($\{f_{ESA} - f_{EPA}\}/f_{EPA}$) in Fig. 7b.

are compared in Fig. 7b and their relative differences (based on the EPA results) are shown in Fig. 7c. It can be seen that the relative difference is within −5–15%.

Figure 8a shows 16 new designs through a randomly chosen path inside the design space box, which is defined as

$$v^j = v_0^j(1 - a^j) + v_1^j a^j, \qquad j = 1, \ldots, 6$$

$$v^1 = \Lambda, \qquad v^2 = \alpha, \qquad v^3 = \tau, \qquad v^4 = A, \qquad v^5 = n_{\text{spar}}$$

$$v^6 = n_{\text{rib}}, \qquad a^j = s^{nj}, \qquad n_j = r_j/(1 - r_j) \qquad (16)$$

where r_j ($j = 1, \ldots, 6$) are randomly determined values between 0 and 1, and see Eq. (15) for the definition of other symbols. Results of natural frequencies of the first six modes for wing structures defined by points along a path with $n_1 = 0.2243$, $n_2 = 0.8591$, $n_3 = 0.2064$, $n_4 = 3.0700$, $n_5 = 2.2196$, and $n_6 = 0.9440$ are shown in Fig. 8b, where it can be seen that results by the EPA and the ESA agree with each other quite well.

Now some static results. For an arbitrary new design whose planform is shown in Fig. 6a, a downward ($-z$ direction) point force of 1 lb is applied at the midpoint of the wing tip. Figure 7b shows displacement components along the leading edge by the EPA and the ESA, compared FEA using MSC/NASTRAN. Figures 7c and 7d show the Von Mises stress distributions at the wing root and the central spanwise line respectively together with the FEA results. Comparison of the natural frequencies of this wing as given by the EPA, the ESA, and the FEA is shown in Table 1. It can be seen that the EPA and the ESA results are close, and they all agree quite well with the FEA results.

Design Space III

In this case a wing plan with $\Lambda = 30$ deg, $s = 192$ in., $b = 72$ in., and $a = 36$ in. (see Fig. 2 for definitions of s, b, and a) is used. A $2^4 \times 3^2$ full factorial experimental design with two levels in t_{0t} (skin thickness at wing tip), a_{rt} (skin-thickness increment ratio at root over the tip), h_1 (spar cap height), and h_2 (rib cap height), and three levels in n_{spar} and n_{rib}, is carried out. The skins are assumed to vary linearly from the root to the tip. Particulars of design space III are as follows:

$$t_{0t} = \{1, 3\} \times 0.118\,\text{in.}, \qquad a_{\text{rt}} = \{0, 2\}$$

$$h_1 = \{1, 3\} \times 0.197\,\text{in.}, \qquad h_2 = \{1, 3\} \times 0.197\,\text{in.}$$

$$n_{\text{spar}} = \{2, 4, 6\}, \qquad n_{\text{rib}} = \{6, 10, 14\}$$

There are 144 sets of data for training. Generating these data sets used much less CPU time than in the case of design space II (about 30 hours). A set of results are given in Fig. 9, where 16 points were randomly chosen within the design space box. The planforms of the new designs are shown in Fig. 9a, where dashed lines indicate the spar or rib positions, and the skin thickness at the wing root and tip, and cap heights of spars and ribs are represented as shown in Fig. 10a. The first 10 natural frequencies by the EPA and the ESA are compared in Fig. 9b, and their relative differences (based on the EPA results) are shown in Fig. 9c. It can be seen that the relative difference is within −5–15%.

Figure 11a shows 16 new designs through a randomly chosen path inside the design space box, which is defined as

$$v^j = v_0^j(1 - a^j) + v_1^j a^j, \qquad j = 1, \ldots, 6$$

$$v^1 = t_{0t}, \qquad v^2 = a_{\text{rt}}, \qquad v^3 = h_1, \qquad v^4 = h_2, \qquad v^5 = n_{\text{spar}}$$

$$v^6 = n_{\text{rib}}, \qquad a^j = s^{n_j}, \qquad n_j = r_j/(1 - r_j) \qquad (17)$$

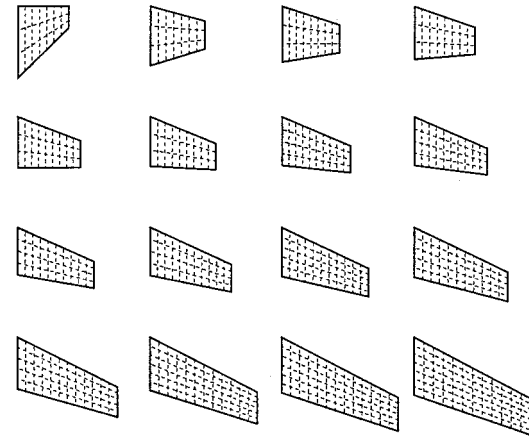

Fig. 8a Sixteen wing planforms systematically varying through design space II.

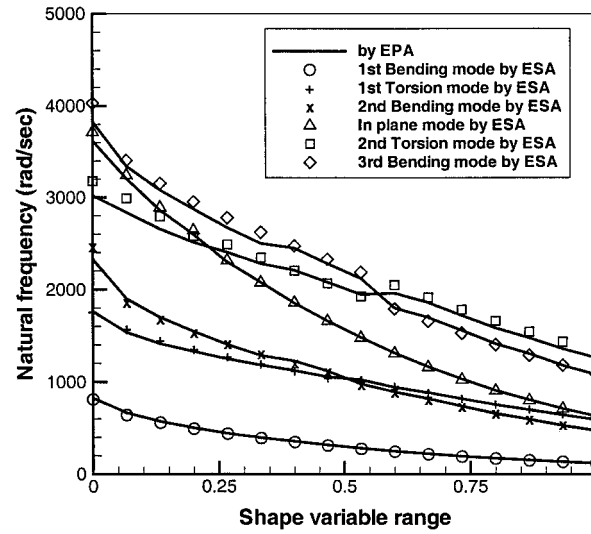

Fig. 8b Comparison of the first six frequencies by EPA and ESA.

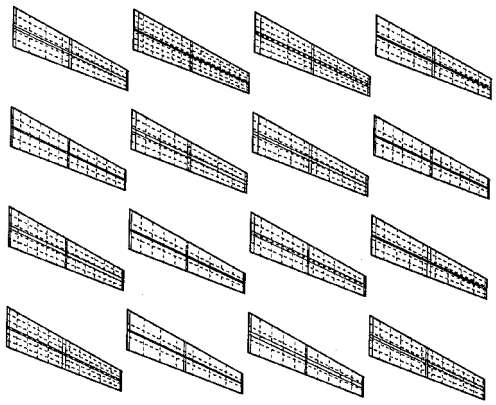

Fig. 9a Sixteen randomly chosen wing designs in design space III.

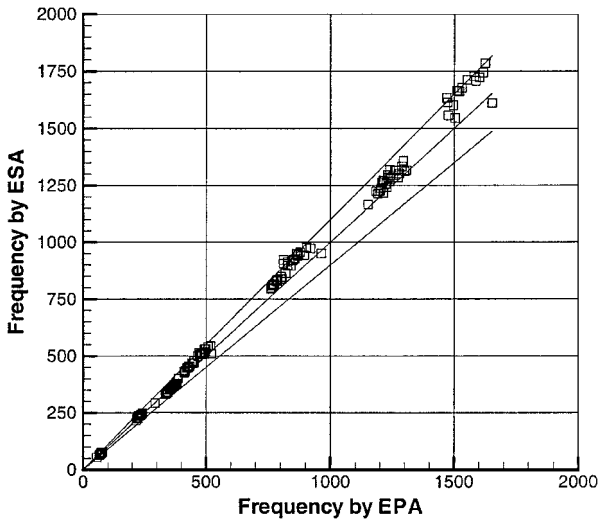

Fig. 9b Comparison of the first 10 frequencies by EPA and ESA.

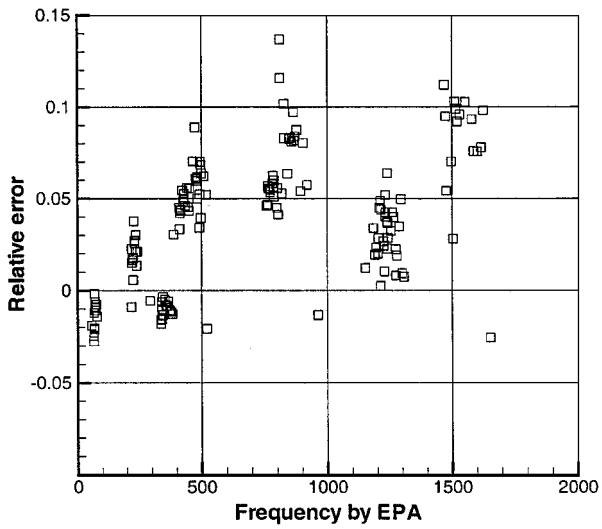

Fig. 9c Relative errors $(\{f_{\mathrm{ESA}} - f_{\mathrm{EPA}}\}/f_{\mathrm{EPA}})$ in Fig. 9b.

where r_j $(j = 1, \ldots, 6)$ are randomly determined values between 0 and 1, and see Eq. (15) for the definition of other symbols. Results of natural frequencies of the first six modes for wing structures defined by points along the path with $n_1 = 0.0031$, $n_2 = 0.9999$, $n_3 = 0.2089, n_4 = 64.7024, n_5 = 0.9067$, and $n_6 = 0.5325$ are shown in Fig. 11b, where it can be seen that results by the EPA and the ESA agree with each other quite well.

For an arbitrary new design whose planform is shown in Fig. 10a, a downward ($-z$ direction) point force of 1 lb is applied at the midpoint of the wing tip. Figure 10b shows displacement components

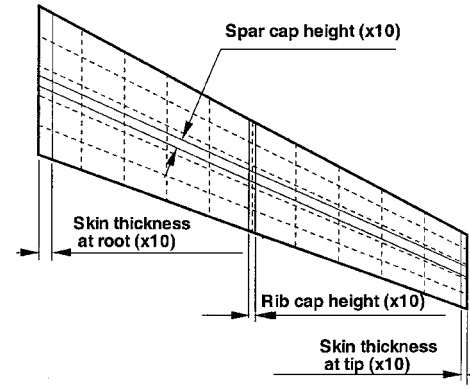

Fig. 10a Arbitrarily chosen wing design in design space III.

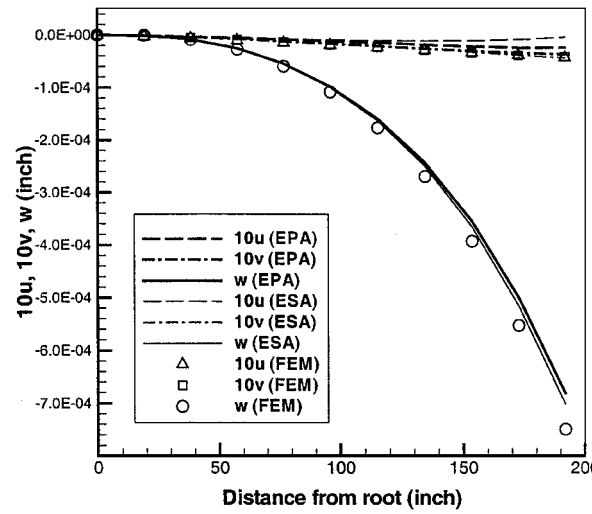

Fig. 10b Comparison of displacements by EPA and ESA under 1-lb tip force.

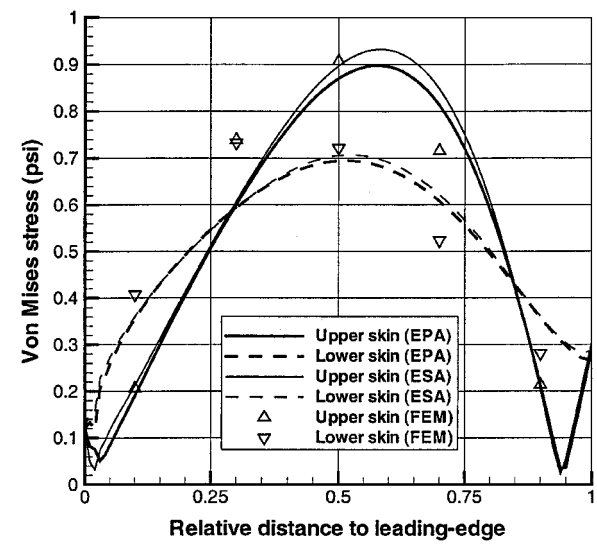

Fig. 10c Comparison of the Von Mises stress at wing root by EPA and ESA under 1-lb tip force.

along the leading edge by the EPA and the ESA, compared with FEA using MSC/NASTRAN. Figures 10c and 10d show the Von Mises stress distributions at the wing root and the central spanwise line respectively together with the FEA results. Comparison of the natural frequencies of this wing as given by the EPA, the ESA, and the FEA is shown in Table 2. Again, it can be seen that the EPA and the ESA results are close, and they all agree quite well with the FEA results. A coarser design space III does not worsen the accuracy of the ESA.

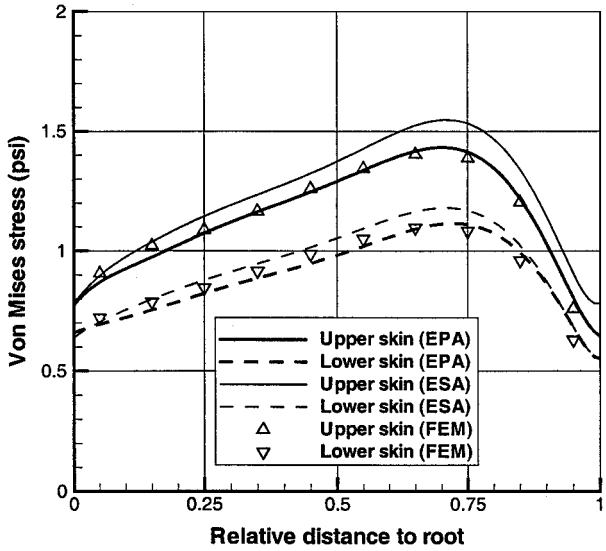

Fig. 10d Comparison of the Von Mises stress along central spanwise line by EPA and ESA under 1-lb tip force.

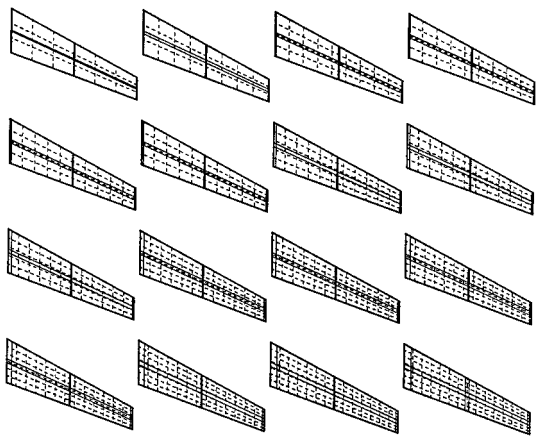

Fig. 11a Sixteen wing designs systematically varying through design space III.

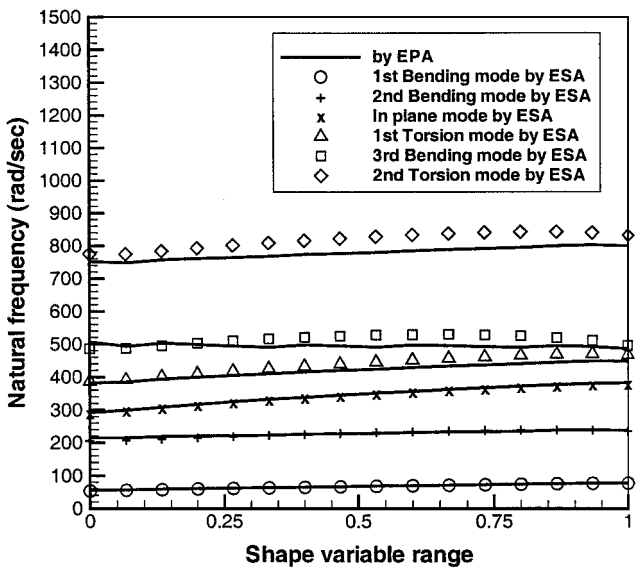

Fig. 11b Comparison of the first six frequencies by EPA and ESA.

Table 2 Natural frequencies of the wing in Fig. 10a

Mode shape and number	Frequency, rad/s		
	EPA	ESA	FEM
1st bending, 1	71.9	70.8	66.0
2nd bending, 2	233.9	239.4	222.6
In plane , 3	358.1	358.4	377.0
1st torsion, 4	452.2	469.4	413.1
3rd bending, 5	479.9	504.8	468.0

The CPU time savings using the ESA were obvious. About 85% less CPU time was spent in evaluating the stiffness and mass matrices compared with the EPA, where matrix evaluation took about 68% of the total CPU time when solving the free vibration problem. Generally speaking, the results given by the ESA in design space II and III were as good as those in design space I although the number of variables increased from four to six.

Although the present ESA can be a good choice to be used as a high-fidelity model for early wing stage design, we lack a direct comparison with some other efficient methods that can "smear" the wing spars and ribs into the skins, such as in the Aeroelastic Tailoring and Structural Optimization (TSO)[4] and Equivalent Laminated Plate Solution (ELAPS).[14] This kind of comparison of methods with different approaches would be very interesting. As to the practice of using NN in the present ESA, it provides an efficient methodology of making use of and accumulating former design experiences and can also be used in any other methods that have a smearing function. This, as suggested by Gunaratnam and Gero,[11] is the real usefulness of neural networks.

Conclusions

An efficient method for the analysis of built-up wing structures using equivalent skin analysis (ESA) has been developed. The CPU time spent on evaluating the matrices, which takes about 63–68% of the total CPU time in the EPA applying to solve a free vibration problem, is about 5–6 times less when the ESA is used. Three groups of examples with four or six design variables show that fairly good results can be obtained. This method is very promising to be used at the early stages of wing design.

Acknowledgments

The authors would like to gratefully acknowledge the support of NASA Langley Research Center for this research through Grant NAG-1-1884 with Jerry Housner and John Wang as the Technical Monitors. Thanks are also given to Eugene Cliff of the Aerospace and Ocean Engineering Department and Tim Tomlin of the Engineering Science and Mechanics Department at Virginia Polytechnic Institute and State University for their assistance in using Crunch, the College of Engineering's SGI Origin 2000 computer.

References

[1] Kapania, R. K., and Liu, Y., "Static and Vibration Analyses of General Wing Structures Using Equivalent Plate Models," *AIAA Journal*, Vol. 38, No. 7, 2000, pp. 1269–1277; also AIAA Paper 2000-1434, April 2000.

[2] Giles, G. L., "Design-Oriented Analysis of Aircraft Fuselage Structures Using Equivalent Plate Methodology," *Journal of Aircraft*, Vol. 36, No. 1, 1999, pp. 21–28.

[3] Livne, E., "Equivalent Plate Structural Modeling for Wing Shape Optimization Including Transverse Shear," *AIAA Journal*, Vol. 32, No. 6, 1994, pp. 1278–1288.

[4] Lynch, R. W., Rogers, W. A., and Brayman, W. W., "Aeroelastic Tailoring of Advanced Composite Structures for Military Aircraft," *AIAA Journal*, Vol.1, 1977; also Air Force Flight Dynamics Lab., AFFDL TR-76-100, Wright–Patterson Air Force Base, OH, 1976.

[5] Kapania, R. K., and Lovejoy, A. E., "Free Vibration of Thick Generally Laminated Cantilever Quadrilateral Plates," *AIAA Journal*, Vol. 34, No. 7, 1996, pp. 1474–1480.

[6] Cortial, F., "Sensitivity of Aeroelastic Response of Wings Using Equivalent Plate Models," Dept. of Aerospace and Ocean Engineering, TR, Virginia Polytechnic Inst. and State Univ., Blacksburg, VA, 1996.

[7] Haykin, S., *Neural Networks: A Comprehensive Foundation*, Macmillan, 1994.

[8]Hajela, P., and Berke, L., "Neurobiological Computational Models in Structural Analysis and Design," *Computers and Structures*, Vol. 41, No. 4, 1991, pp. 657–667.

[9]Abdalla, K. M., and Stavroulakis, G. E., "A Backpropagation Neural Network Model for Semi-Rigid Steel Connections," *Microcomputers in Civil Engineering*, Vol. 10, No. 2, 1995, pp. 77–87.

[10]Vanluchene, R. D., and Sun, R., "Neural Network in Structural Engineering," *Microcomputers in Civil Engineering*, Vol. 5, No. 3, 1990, pp. 207–215.

[11]Gunaratnam, D. J., and Gero, J. S., "Effect of Representation on the Performance of Neural Networks in Structural Engineering Applications," *Microcomputers in Civil Engineering*, Vol. 9, No. 2, 1994, pp. 97–108.

[12]Liu, Y., Kapania, R., and VanLandingham, H., "Simulating and Synthesizing Substructures Using Neural Network and Genetic Algorithms," *Modeling and Simulation Based Engineering*, edited by S. N. Atluri and P. E. O'Donoghue, Vol. I, Tech Science Press, Palmdale, CA, 1998, pp. 576–581.

[13]Karamcheti, K., *Principles of Ideal-Fluid Aerodynamics*, R. E. Krieger, New York, 1980.

[14]Giles, G. L., "Equivalent Plate Modeling for Conceptual Design of Aircraft Wing Structures," AIAA Paper 95-3945, Dec. 1995.

E. Livne
Associate Editor